



PERGAMON

Journal of Quantitative Spectroscopy &
Radiative Transfer 78 (2003) 171–178

Journal of
Quantitative
Spectroscopy &
Radiative
Transfer

www.elsevier.com/locate/jqsrt

Cavity ring-down measurement of the O₂–O₂ collision-induced absorption resonance at 477 nm at sub-atmospheric pressures

Maarten Sneepe*, Wim Ubachs

*Department of Physics and Astronomy, Laser Centre, Vrije Universiteit, De Boelelaan 1081,
1081 HV, Amsterdam, The Netherlands*

Received 11 June 2002; received in revised form 13 August 2002; accepted 14 August 2002

Abstract

The collision-induced absorption feature $X^3\Sigma_g^-(v=0) + X^3\Sigma_g^-(v=0) \rightarrow a^1\Delta_g(v=0) + b^1\Sigma_g^+(v=0)$ in the wavelength range 467–490 nm has been investigated by means of the laser-based cavity-ring-down technique at pressures between 0 and 1000 hPa and at $T = 294$ K. Pressure and wavelength dependent cross sections have been determined leading to a band-integrated value of $(2.18 \pm 0.04) \times 10^{-43}$ cm⁴ molecule⁻². Special care has been given to the wings of the resonance profile and the Rayleigh extinction was taken into account. © 2003 Elsevier Science Ltd. All rights reserved.

Keywords: Collision-induced absorption; Oxygen

1. Introduction

The O₂-dimer complexes are interesting in molecular physics as well as from an atmospheric perspective. Already in the early studies on liquid oxygen by Ellis and Kneser [1], it was understood that the observed broad resonances were related to simultaneous excitation of two O₂ molecules into a vibronically excited state, as a result of absorption of a single photon. Also the correct assignment in terms of quantum numbers was established as early as 1933 [1], i.e. not long after the advent of molecular quantum mechanics. The resonance at 477 nm, investigated in this study, can be assigned as a simultaneous excitation of two ground state oxygen molecules, one into the $a^1\Delta_g(v=0)$ state and one into $b^1\Sigma_g^+(v=0)$.

In the literature on the O₂–O₂ features there has been some dispute on whether the absorption is due to true dimers, i.e. bound Van der Waals complexes, or to pairs of unbound O₂ molecules

* Corresponding author. Tel.: +31-20-444-7950; fax: +31-20-444-7999.

E-mail addresses: sneepe@nat.vu.nl (M. Sneepe), wimu@nat.vu.nl (W. Ubachs).

during a collisional fly-by. Ripple structure, observed by Long and Ewing [2] at low temperatures indicated that bound complexes play a role in the absorption. Ab initio calculations predict a well depth of some 150 cm^{-1} [3], supporting a large number of bound states. Molecular beam scattering studies by Aquilanti et al. [4] have unequivocally proven the existence of bound dimers in the ground state. The slit-jet cavity ring-down studies by Campargue et al. [5] revealed extremely narrow absorption features of $(\text{O}_2)_2$ in the 630 and 580 nm bands. This proves that Van der Waals complexes, consisting of two $a^1\Delta_g(v=0)$ excited oxygen molecules, are long-lived on the time-scale of the experiment and are resistant to predissociation. It may be expected that this situation also holds for the $a^1\Delta_g(v=0) + b^1\Sigma_g^+(v=0)$ complex and that narrow transitions play a role. However, at room temperature the partition function is dominated by the dissociative continuum of the complex and the phenomenon of collision-induced or free-free absorption will dominate the 477 nm resonance feature of oxygen.

The features associated with $\text{O}_2\text{--O}_2$ collisional complexes have attracted much interest in atmospheric physics. Pfeilsticker et al. [6] and Solomon et al. [7] have evaluated the role of O_4 as an absorber of solar radiation, and concluded that the globally averaged all-sky absorption by collision complexes of oxygen is likely to be between 0.9 and 1.3 W m^{-2} (including the $\text{N}_2\text{--O}_2$ complex at $1.26 \mu\text{m}$). Moreover, in view of its quadratic dependence on pressure, the $(\text{O}_2)_2$ features can be used in remote sensing applications, e.g. in the determination of cloud top heights from satellite data [8]. Recently in situ atmospheric measurements were performed on the UV/vis $\text{O}_2\text{--O}_2$ bands yielding the result that absorption profiles are independent of pressure and temperature in the range of relevance for the atmosphere [9]. Moreover, the values for the cross section are consistent with those obtained from high pressure (55 bar) measurements by Greenblatt et al. [10]. From the in situ data a value for the formation enthalpy of the bound $\text{O}_2\text{--O}_2$ dimers could be deduced. The red (630 nm) and yellow (580 nm) bands are the strongest and would in principle be most useful for remote sensing purposes, if it were not for the fact that these features are overlaid by other absorption features: the O_2 γ -band in the red and a water vapor absorption band in the yellow, which is itself used for satellite data retrieval [11]. The blue feature at 477 nm is easily traceable in atmospheric observation since inferring absorptions from other gases, e.g. O_3 , NO_2 and H_2O are either weak (NO_2 and H_2O) or more identifiable through neighboring bands. For this reason accurate measurement by an alternative technique is warranted.

Since the early studies in the 1930s in the liquid [1] and gaseous phase [12] a number of laboratory investigations have been performed to determine the absorption strengths of the collision-induced $\text{O}_2\text{--O}_2$ features [2,10,13–15]. But in view of the weakness of the bands pressures above or at atmospheric pressure were used to spectrally record the features. In this paper we report on the use of cavity-ring down (CRD) laser spectroscopic technique applied to the blue $(\text{O}_2)_2$ system at sub-atmospheric pressures as a follow-up to studies on the red and yellow features [16].

2. Experiment and results

The experimental setup and methods reflect those used in a previous study [16] except for a change of wavelength. The interval 467–490 nm was covered by running a Quanta-Ray PDL-3 pulsed dye laser system (bandwidth 0.05 cm^{-1}) on Coumarine-480 dye, which was pumped by the 355 nm output of a pulsed Nd:YAG laser. A stable, non-confocal resonator of length 82 cm is formed by

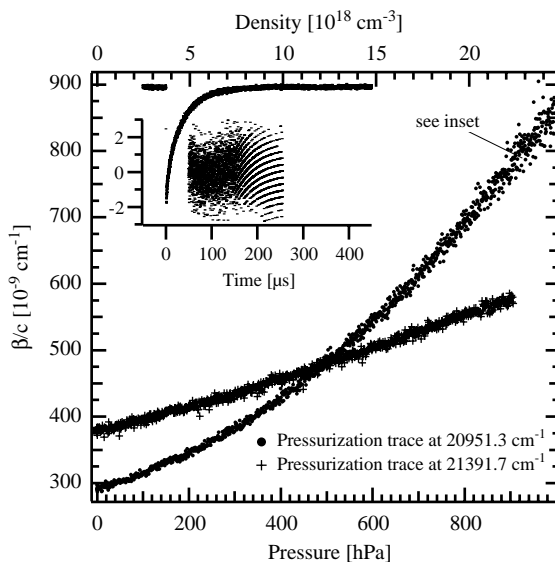


Fig. 1. Two typical pressurization traces. The offset β_c^0 on the vertical axis shows the difference in reflectivity between the two wavelengths. The inset shows a ringdown transient (negative peak) and the residuals of the single exponential fit (“fingerprint” pattern). The trace was taken from the pressurization trace at 20951.3 cm^{-1} , near the end of the trace, the location is indicated with a label. The residuals show clear signs of digitization noise, especially near the end. The fitting algorithm stops the fitting procedure in that case. This leads to increased noise-levels near the end of the pressurization trace. Note that the vertical scale of the inset is for the residuals, the ringdown transient itself has no scale.

mirrors of reflectivity $\geq 99.994\%$ over the investigated frequency range and radius of curvature of 100 cm.

The $\text{O}_2\text{-O}_2$ resonance was recorded in discrete steps, whereby for each position the frequency was measured with an echelle-grating spectrograph, yielding an accuracy of 0.2 cm^{-1} . While keeping the frequency fixed at a certain value, pulsed CRD-transients were measured continuously at a repetition rate of 10 Hz, and oxygen gas was slowly flushed into the CRD-cell. The inlet-flow was controlled by a needle valve, set to cover a time period of 15–20 min for full pressurization up to 1000 hPa. A filter with $0.5 \mu\text{m}$ pores was used to extract aerosols from the oxygen gas. Oxygen with a purity of 99.5% was used without further purification. Two typical pressurization traces are shown in Fig. 1.

The traces consist of about 1100 data points, with each point recorded at a certain pressure, which was measured on-line by a capacitance baratron with an uncertainty of 2 hPa. The pressure and the simultaneously measured temperature were used to calculate the density of the gas, using the ideal gas law, assumed to introduce only a negligible error at these pressures and temperatures. Each data point in Fig. 1 is a result of a fit to a ring-down transient which is detected by a photomultiplier, digitized by an 8-bits oscilloscope (Lecroy waverunner LT 342, used at a sample speed of 20 MS/s) and finally transferred to a computer for further analysis. The loss rate per unit time ($\beta_c(n)$) depends on the density n . This loss rate follows from a non-linear least-squares fit to the recorded transients, using a single exponential function and a determination of the base-line.

As was demonstrated by Naus et al. [17] the ring-down transients from a generic pulsed CRD-experiment can be straightforwardly interpreted as an absorption strength or cross section under the condition that the transients are mono-exponential. Then the loss-rate equals:

$$\beta_{\lambda}(n) = \beta_{\lambda}^0 + \tilde{\alpha}_{\lambda, \text{tot}}(n)c, \quad (1)$$

where c is the speed of light and β_{λ}^0 the frequency-dependent loss rate due to the limited and frequency-dependent reflectivity of the mirrors. In this work the procedure was followed to optimize the alignment of the ring-down cavity to produce mono-exponential decays by on-line monitoring of a variance parameter defined in Ref. [17]. The fitting procedure to yield $\beta_{\lambda}(n)$ from the observed transients was done in a two-step fashion. In a first step a non-weighted fit was performed, while in a second step, a weighted fit-procedure was followed, using the weights derived in the first round of fitting. As discussed in Ref. [17] in this way the information content of the CRD-transients is optimally used and a true statistical uncertainty to the result can be given. In the wavelength domain 467–490 nm, 53 pressurization curves were measured, two of which are displayed in Fig. 1. These curves can be parametrized by three parameters

$$\beta_{\lambda}(n) = \beta_{\lambda}^0 + \sigma_{\lambda}^{\text{R}}nc + \alpha_{\lambda}^{\text{q}}n^2c. \quad (2)$$

The linear component $\sigma_{\lambda}^{\text{R}}$ in Eq. (2) is the Rayleigh scattering cross section. This value can be computed from the refractive index and the depolarization ratio, see Ref. [18]. The refractive indices and King correction factor were taken from Ref. [19]. We kept $\sigma_{\lambda}^{\text{R}}$ fixed to the computed value of the Rayleigh scattering cross section in our least-squares fit of the remaining two parameters β_{λ}^0 and $\alpha_{\lambda}^{\text{q}}$ to the measured pressure-ramp. The β_{λ}^0 parameter gives information about the reflectivity of the mirrors. The $\alpha_{\lambda}^{\text{q}}$ parameter, representing the quadratic pressure dependence is plotted in Fig. 2 for the 467–490 nm interval. The function used to create the fit shown in the same figure, is discussed in Section 3.

During the analysis of our data we verified that the $\sigma_{\lambda}^{\text{R}}$ parameter, if calculated from the fit, had the expected value. The values we found were very close, but the correlation between $\sigma_{\lambda}^{\text{R}}$ and $\alpha_{\lambda}^{\text{q}}$ was relatively high. We therefore used a fit with a calculated and fixed value of $\sigma_{\lambda}^{\text{R}}$, which gave us a better estimate of the O₂–O₂ contribution.

3. The model-equation for the profile

The O₂–O₂ absorption is complex and involves two multi-dimensional potential energy surfaces. There is no simple expression that describes the profile; all possible contributions from bound and free states on the ground and excited state potential surfaces have to be included, weighted by their proper Boltzmann population factors and kinetic energies. A simplified, empirical picture that turns out to describe the O₂–O₂ collision induced transition fairly well, was suggested by Watanabe and Welsh [20] and later used by several others [21,22,14]. We will follow this treatment.

Individual collision-induced transitions exhibit a Boltzmann relation between the intensities in the high- and low-frequency wings. One could consider this as if the kinetic energy of the molecules that take part in the absorption can compensate a shortage of energy in the photon to make the

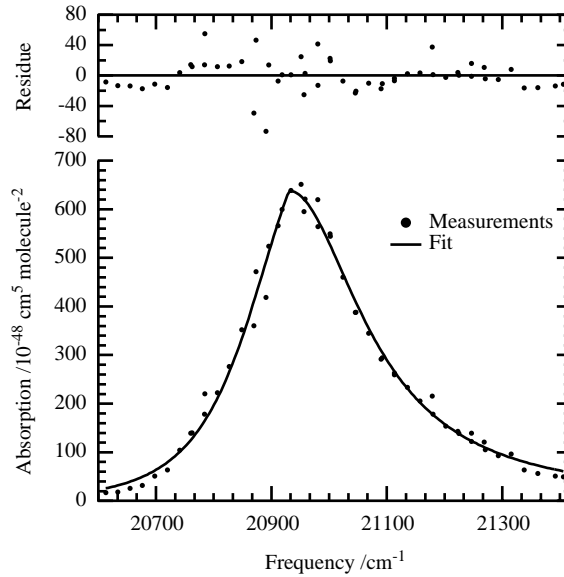


Fig. 2. The absorption profile. The bottom panel shows the measured points (dots) and the fit to these points (drawn line) The function used for the fit is discussed in Section 3. The top panel shows the difference between the fit and the measured points. The vertical scale on both is the same.

double transition. This may be represented by

$$\frac{\mathcal{A}(v_c - \Delta v)}{\mathcal{A}(v_c + \Delta v)} = \exp \left[-\frac{hc\Delta v}{k_B T} \right] \quad (3)$$

with \mathcal{A} the intensity of the absorption, v_c the central position of the absorption, $\Delta v = v - v_c$, T the temperature of the gas, and h , c and k_B are Planck’s constant, the speed of light and Boltzmann’s constant, respectively.

Eq (3) gives the ratio between the high- and low-frequency wings, but it does not specify the shape of the line itself. The basic profile is a Lorentzian profile, where the lower energy side is modified to reflect the fraction of molecules which have an energy high enough to contribute to the absorption. This leads to

$$\mathcal{A} = \frac{a(\Gamma/2)^2}{(\Delta v)^2 + (\Gamma/2)^2} \times \begin{cases} 1 & \text{if } \Delta v > 0, \\ \exp(hc\Delta v/k_B T) & \text{if } \Delta v \leq 0, \end{cases} \quad (4)$$

where a and Γ are parameters for the amplitude and the width of the absorption, respectively.

The model equation as given by Eq. (4) is fitted to the intensities α_λ^q , found in the first fit of the loss-rate during a pressure ramp to Eq. (2). The results of this final fit are shown in Table 1. To find the integrated cross section, the model equation is integrated, using the parameters found in the fit. The final width parameter one would designate as the FWHM width is of course different, since the cutoff by the exponent is not included in Γ . The cutoff by the Boltzmann factor also causes our results to be shifted slightly towards lower frequencies, with respect to previous studies. This is a direct consequence of the treatment of the absorption profile as asymmetric. A comparison with

Table 1
Parameters found using Eq. (4) as the model function and a least-squares fit

Parameter	Measured value
ν_c	$20930.5 \pm 1.6 \text{ cm}^{-1}$
λ_c	$477.77 \pm 0.07 \text{ nm}$
FWHM	$241 \pm 7 \text{ cm}^{-1}$
FWHM	$5.50 \pm 0.01 \text{ nm}$
Γ	$309 \pm 7 \text{ cm}^{-1}$
a	$(6.38 \pm 0.16) \times 10^{-46} \text{ cm}^5 \text{ molecule}^{-2}$
$\int \mathcal{A} \, d\nu$	$(2.18 \pm 0.04) \times 10^{-43} \text{ cm}^4 \text{ molecule}^{-2}$

The indicated errors are 1σ values. A graphical representation of the data and the fit-result can be seen in Fig. 2.

Table 2
A comparison between literature values and our results

Reference	$\int_{\text{Band}} \mathcal{A} \, d\nu$ ($\text{cm}^4 \text{ molecule}^{-2}$)	Peak height ($\text{cm}^5 \text{ molecule}^{-2}$)	Width (cm^{-1})	Density (amagat^a)
Tabisz et al. [21]	2.09×10^{-43}	7.3×10^{-46}	200	100–300
Blickensderfer et al. [23]	$2.4 \pm 0.4 \times 10^{-43}$	7.1×10^{-46}	300 ± 40	2–4
McKellar et al. [14]	2.20×10^{-43}	6.4×10^{-46}	— ^b	4.4
Greenblatt et al. [10]	— ^b	$6.3 \pm 0.6 \times 10^{-46}$	270	1–55 bar
Newnham et al. [15]	$2.483 \pm 0.048 \times 10^{-43}$	$8.34 \pm 0.83 \times 10^{-46}$	— ^b	1000 hPa
This work	$2.18 \pm 0.04 \times 10^{-43}$	$6.38 \pm 0.16 \times 10^{-46}$	241 ± 7	0–1000 hPa

^aDimensionless density, relative to the density at 273.15 K and 101,325 Pa.

^bNot indicated.

previous studies is included in Table 2. The results of McKellar et al. [14], initially in terms of a cross section divided by the frequency of the transition, were recalculated in the presently used units for comparison. When comparing all results collected in Table 2 there appears a consistency with a gradual trend toward higher accuracy in the obtained band parameters, with the exception however of the values reported in Ref. [15], that deviate substantially, particularly in view of the stated error margins.

4. Conclusion

Cavity ring-down spectroscopy has been used to determine the band parameters of the $X^3\Sigma_g^-(v=0) + X^3\Sigma_g^-(v=0) \rightarrow a^1\Delta_g(v=0) + b^1\Sigma_g^+(v=0)$ absorption feature in a pressure range from 0 to 1000 hPa. In the analysis it was verified that the collision-induced absorption of oxygen is a quadratic function of pressure, and Rayleigh extinction was taken into account. For the final results the Rayleigh cross section was set to the computed value, but earlier analysis showed that the linear component in the loss-rate (see Eq. (2)) compares favorably to the theoretical value. Care has been

taken to align the ring-down cavity correctly, so that the decay transient can be interpreted as a single exponential decay, yielding correct cross sections.

The presently derived parameters describing the blue (O₂)₂ feature are consistent with the body of previously obtained values, while the accuracy is better. The data may be of use for data retrieval by satellite instruments spectrally covering the blue range, such as in the case of the Ozon Monitoring Instrument (OMI), which is currently under development.

Acknowledgements

The present work was supported by the Space Research Organization Netherlands (SRON) with a grant (EO-036) in the Earth Observation program. The authors wish to thank I. Aben (SRON), P.F. Levelt (KNMI, OMI-project), G. Tabisz (Univ. Manitoba), A. McKellar (NRC Ottawa) and L. Frommhold (Univ. Texas) for fruitful discussions.

References

- [1] Ellis JW, Kneser HO. Kombinationsbeziehungen im Absorptionsspektrum des flüssigen Sauerstoffes. *Z Phys* 1933;86:583–91.
- [2] Long CA, Ewing GE. Spectroscopic investigation of van der Waals molecules. I. The infrared and visible spectra of O₄. *J Chem Phys* 1973;58:4824–34.
- [3] Wormer PES, van der Avoird A. (Heisenberg)exchange and electrostatic interactions between O₂ molecules: An ab initio study. *J Chem Phys* 1984;81:1929–40.
- [4] Aquilanti V, Ascenzi D, Bartolomei M, Cappelletti D, Cavalli S, Vitores MD, Pirani F. Molecular beam scattering of aligned oxygen molecules. The nature of the bond in the O₂–O₂ dimer. *J Am Chem Soc* 1999;121:10,794–802.
- [5] Campargue A, Biennier L, Kachanov A, Jost R, Bussery-Honvault B, Veyret V, Churrassy S, Bacis R. Rotationally resolved absorption spectrum of the O₂ dimer in the visible range. *Chem Phys Lett* 1998;288:734–42.
- [6] Pfeilsticker K, Erle F, Platt U. Absorption of solar radiation by atmospheric O₄. *J Atmos Sci* 1997;54:933–9.
- [7] Solomon S, Portmann RW, Sanders RW, Daniel JS. Absorption of solar radiation by water vapor, oxygen and related collision pairs in the Earth's atmosphere. *J Geophys Res* 1998;104:3847–58.
- [8] Erle F, Pfeilsticker K, Platt U. On the influence of tropospheric clouds on zenith-scattered-light measurements of stratospheric species. *Geophys Res Lett* 1995;22:2725–8.
- [9] Pfeilsticker K, Bösch H, Camy-Peyret C, Fitzenberger R, Harder H, Osterkamp H. First atmospheric profile measurements of UV/visible O₄ absorption band intensities: implications for the spectroscopy, and the formation enthalpy of the O₂–O₂ dimer. *Geophys Res Lett* 2001;28:4595–8.
- [10] Greenblatt GD, Orlando JJ, Burkholder JB, Ravishankara AR. Absorption measurements of oxygen between 330 and 1140 nm. *J Geophys Res* 1990;95:18,577–82.
- [11] Maurellis AN, Lang R, van der Zande W, Aben I, Ubachs W. Precipitable water column retrieval from GOME data. *Geophys Res Lett* 2000;27:903–6.
- [12] Salow H, Steiner W. Die durch Wechselwirkungskräfte bedingten Absorptionsspektren des Sauerstoffes, 1. Die Absorptionsbanden des (O₂–O₂)-Moleküls. *Z Physik* 1936;99:137–58.
- [13] Dianov-Klokov VI. Absorption spectrum of oxygen at pressures from 2 to 35 atm in the region 12,600 to 3600 Å. *Opt Spectrosc* 1964;16:224–7.
- [14] McKellar ARW, Rich NH, Welsh HL. Collision-induced vibrational and electronic spectra of gaseous oxygen at low temperatures. *Can J Phys* 1972;50:1–9.
- [15] Newnham DA, Ballard J. Visible absorption cross sections and integrated absorption intensities of molecular oxygen (O₂ and O₄). *J Geophys Res* 1998;103:28,801–16.
- [16] Naus H, Ubachs W. Visible absorption bands of the O₄ collision complex at pressures below 760 Torr. *Appl Opt* 1999;38:3423–8.

- [17] Naus H, van Stokkum IHM, Hogervorst W, Ubachs W. Quantitative analysis of decay transients applied to a multimode pulsed cavity ringdown experiment. *Appl Opt* 2001;40:4416–26.
- [18] Bucholtz A. Rayleigh-scattering calculations for the terrestrial atmosphere. *Appl Opt* 1995;34:2765–73.
- [19] Bates DR. Rayleigh scattering by air. *Planet Space Sci* 1984;32:785–90.
- [20] Watanabe A, Welsh HL. Pressure-induced infrared absorption of gaseous hydrogen and deuterium at low temperatures II. Analysis of the band profiles for hydrogen. *Can J Phys* 1967;45:2859–71.
- [21] Tabisz GC, Allen EJ, Welsh HL. Interpretation of the visible and near-infrared absorption spectra of compressed oxygen as collision-induced electronic transitions. *Can J Phys* 1969;47:2859–71.
- [22] Blickensderfer RP, Ewing GE. Collision-induced absorption spectrum of gaseous oxygen at low temperatures and pressures. I. The ${}^1\Delta_g \leftarrow {}^3\Sigma_g^+$ System. *J Chem Phys* 1969;51:873–83.
- [23] Blickensderfer RP, Ewing GE. Collision-induced absorption spectrum of gaseous oxygen at low temperatures and pressures. II. The simultaneous transitions ${}^1\Delta_g + {}^1\Delta_g \leftarrow {}^3\Sigma_g^- + {}^3\Sigma_g^-$ and ${}^1\Delta_g + {}^3\Sigma_g^- \leftarrow {}^3\Sigma_g^- + {}^3\Sigma_g^-$. *J Chem Phys* 1969;51:5284–9.